MATERIALS SCIENCE

Direct link between mechanical stability in gels and percolation of isostatic particles

Hideyo Tsurusawa[1]*, Mathieu Leocmach[2]*, John Russo[1,3], Hajime Tanaka[1]†

Colloidal gels have unique mechanical and transport properties that stem from their bicontinuous nature, in which a colloidal network is intertwined with a viscous solvent, and have found numerous applications in foods, cosmetics, and construction materials and for medical applications, such as cartilage replacements. So far, our understanding of the process of colloidal gelation is limited to long-time dynamical effects, where gelation is viewed as a phase separation process interrupted by the glass transition. However, this purely out-of-equilibrium thermodynamic picture does not address the emergence of mechanical stability. With confocal microscopy experiments, we reveal that mechanical metastability is reached only after isotropic percolation of locally isostatic environments, establishing a direct link between the load-bearing ability of gels and the isostaticity condition. Our work suggests an operative description of gels based on mechanical equilibrium and isostaticity, providing the physical basis for the stability and rheology of these materials.

INTRODUCTION

Colloidal gels are soft solids composed of two intertwined phases: a solid network and a liquid solvent. They are a ubiquitous state of matter in everyday life, making up most of the foods we eat, the cosmetics we use, concretes, and our own organs. In colloidal gels, the network is composed of colloidal particles bonded together by attractive forces. These colloidal assemblies are out of equilibrium, as the thermodynamic ground state of the system involves the macroscopic separation between a particle-rich (liquid) and a particle-poor (gas) phase. Despite the thermodynamic driving force toward compactness, the gel persists because of the dynamical arrest of the network, often described as a glass transition (*1*–*8*). This has led to the popular physical picture that a gel is formed by dynamical arrest of bicontinuous spinodal decomposition due to glass transition. The direct link between spontaneous gelation and spinodal decomposition has been carefully confirmed by combining experiments and theories (*8*). This recently established scenario is certainly a large step toward a more complete understanding of colloidal gelation.

However, this picture still leaves some fundamental problems unanswered: (i) The knowledge of ordinary spinodal decomposition predicts that the minority colloid-rich phase should form isolated clusters rather than the observed percolated network (*9*). (ii) A colloidal gel is sometimes formed by a network made of thin arms, which are too thin to be regarded as glasses. This casts some doubt on the popular scenario of dynamic arrest due to a glass transition. The glass transition is defined as a kinetic transition and has no direct link to mechanical stability in a strict sense. Slow dynamics and mechanical stability are conceptually different. In an extreme case, for example, a gel formed by bonds with a short lifetime can be ergodic and in an equilibrium state. (iii) A gel often displays superdiffusive behavior, detected as the compressed exponential decay of a density correlation function, during aging, as observed by time-resolved spectroscopy techniques (*10*–*12*) and, recently, simulations (*13*–*15*). The origin of this phenomenon and its relation to problem (ii) are still elusive.

Several mechanisms have been proposed to try to rationalize some of these issues. Fluid momentum conservation can play an important role in phase separation of colloidal suspensions, giving to hydrodynamics an active role in network formation of the colloid-rich phase (*4*, *16*). There have been some numerical studies on the role of hydrodynamics (*17*, *18*) and mechanics (*10*, *13*, *15*, *19*–*21*) in colloidal gelation. However, experimental investigations of these problems have been limited to observation of gels already formed (*22*, *23*) because of the lack of a method to follow the whole kinetic processes with single-particle resolution in both space and time.

Moreover, some questions on the emergence of elasticity, which is the most fundamental physical property of gels, have still remained unanswered. It is well known that the isotropic percolation of a bond network is not sufficient to ensure mechanical stability (*23*–*25*). The stability of gels is ascribed to the formation of locally favored structures or local energy-minimum configurations (*26*), while the mechanics of the network is being recognized to play a major role in the aging behavior of gels (*13*, *14*, *27*, *28*). Purely geometrical conditions for mechanical stability have also been proposed. Whether a network is rigid can be determined using a pebble game algorithm (*29*), but this method is limited to two-dimensional systems (*30*). A criterion on the average coordination number has been proposed (*24*) but has been recently invalidated (*23*). Kohl *et al.* (*23*) found that in dilute suspensions, a final gel state is obtained only after directed percolation was observed, which differs from isotropic percolation by taking into account the directionality of the clusters. Hsiao *et al.* (*31*) found that strain-induced yielding coincides with the loss of rigid clusters. Rigidity was defined using a local Maxwell criterion for isostaticity, that is, six neighbors per particle (*32*, *33*). However, the relationship between local structures, dynamic arrest, and the emergence of elasticity remains poorly understood even at a fundamental level.

This issue is also related to the fundamental problem of distinguishing colloidal gels and glasses. In general, colloidal systems form two types of non-ergodic disordered states (*34*, *35*), gels and glasses [hard sphere–like glasses (*36*), Wigner glasses (*37*, *38*), and attractive glasses (*39*)], depending on the type of interactions and volume fractions. It is not

[1]Department of Fundamental Engineering, Institute of Industrial Science, University of Tokyo, 4-6-1 Komaba, Meguro-ku, Tokyo 153-8505, Japan. [2]Université de Lyon, Université Claude Bernard Lyon 1, CNRS, Institut Lumière Matière, F-69622 Villeurbanne, France. [3]School of Mathematics, University of Bristol, Bristol BS8 1TW, UK.
*These authors contributed equally to this work.
†Corresponding author. Email: tanaka@iis.u-tokyo.ac.jp.

straightforward to distinguish Wigner glasses and gels when long-range repulsion and short-range attraction are competing at low volume fractions (*40*, *41*). A similar situation arises for gels and attractive glasses with short-range attractions at high volume fractions (*42*). The above difficulty in distinguishing gels and glasses conceptually originates from the picture that the non-ergodicity of gels emerges from dynamic arrest due to glass transition.

To address these problems, here, we study the role of mechanics in colloidal gelation by dynamical confocal microscopy experiments. Various experimental protocols have been proposed to obtain reproducible gel structures from the micrometer-sized particles necessary for particle-level resolution. Most of them involved shear (*43*–*46*), but, here, we use a protocol that does not involve external flow and that allows us to observe the entire gelation process, from the beginning to the end with particle-level resolution. Our results point to the crucial role of isostatic structures, which are clusters of particles that, according to the Maxwell criteria of stability, have a number of neighbors equal to the number of degrees of freedom. We observe that the emergence of solidity coincides with the appearance of a system-spanning cluster of isostatic particles, i.e., with the isotropic percolation of isostatic particles. Both the glass transition and directed percolation are necessary, but not sufficient, conditions for the emergence of mechanical metastability. In relation to this, we show that directed percolation and isotropic percolation of isostatic particles happen simultaneously only in dilute systems, while in concentrated systems, the two time scales decouple, allowing us to link rigidity with the appearance of the system-spanning cluster of isostatic particles. These findings shed new light on the mechanisms of gel formation and coarsening and also on the fate of gels.

RESULTS

Phase separation dynamics observed at a single-particle level

System design

In our protocol, we first enclose a salt-free suspension of sterically and charge-stabilized colloids and nonadsorbing polymers in a thin microscopy cell sketched in fig. S1. The bottom wall of the cell is an osmotic membrane providing contact with a long channel full of the same solvent mixture. Salt dissolution and subsequent migration of the ions along the channel and through the membrane induce screening of the electrostatic repulsion, revealing the depletion potential well due to the polymers. In contrast to similar designs used in our group and by others (*47*–*49*), here, the time needed for the ions to diffuse from the membrane across the cell thickness is of the same order of magnitude as the Brownian time of the particles $\tau_B = 10$ s. This relation between the two key time scales enables us to switch instantaneously (physically) from a long-range repulsive to a short-range attractive system without any external solvent flow. This causes uniform gelation starting from the homogeneous state, allowing in situ confocal microscopy observation throughout the process from a well-defined initial time, as shown in Fig. 1 and movie S1.

Here, we stress that after the salt concentration is homogenized, our system can be regarded as a standard model for sticky hard sphere systems. We confirmed this by comparing the experimental phase diagram with the one obtained with free-volume theory for sticky hard spheres (Fig. 2).

Phase separation dynamics

In Fig. 2A, we show the phase diagram, where we can divide the state points into three regions based on the final state obtained by our protocol: at low polymer concentration ($c_p < 0.2$ mg/g), a sample fully relaxes to a fluid state; at very low colloid volume fraction ($\phi < 0.05$) and high polymer concentration, the particles condense into long-lived well-separated clusters, as observed in (*50*); and in the rest of the explored phase space, we observe a long-lived space-spanning network. In the phase diagram, we also plot the spinodal line obtained from free-volume theory calculations (*51*) as the continuous and dotted curves for below and above the polymer overlap concentration, respectively. Despite the limitations of the theory, the agreement between the spinodal line and our experiments is rather satisfactory, with the only exception being the region of small colloidal volume fractions and high polymer concentration [see, e.g., (*8*)].

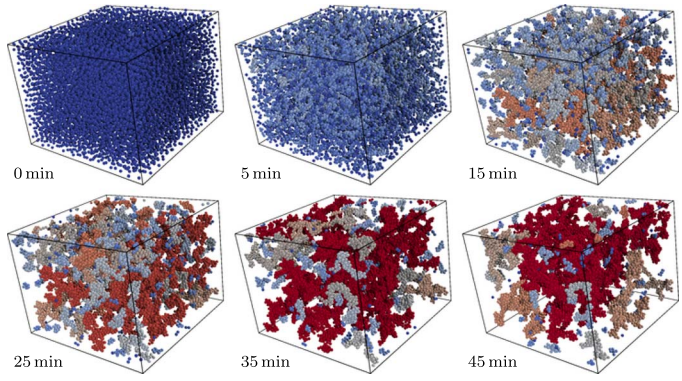

Fig. 1. Snapshots from the entire gelation process reconstructed via particle tracking of a typical sample close to the cluster-gel line ($\phi = 7.5$, $c_p = 1$ mg/g) using the salt injection protocol. Particles are colored according to the size of the cluster they belong to, going from blue for monomers to red for the percolated cluster. See also movie S1.

We confirm in the Supplementary Materials that the phase separation kinetics follows arrested spinodal behavior both in the cluster phase and in the percolating samples. We also confirm in the Supplementary Materials the crucial role of hydrodynamics in facilitating percolation.

To characterize the gelation path in real space, we compute the instantaneous mean number of neighbors $\overline{N}_C$, or coordination number, that quantifies the compactness of the structure. We also compute the spatial extent of the largest cluster l_{max} that we normalize by the size of the field of view L to obtain a measure of the distance to isotropic percolation of the system. Figure 2B shows a system trajectory in the $(l_{max}/L, \overline{N}_C)$ plane for various colloidal volume fractions ϕ. All trajectories show a linear increase of both cluster size l_{max}/L and number of neighbors $\overline{N}_C$ at early times. This is followed by the coarsening stage, which happens differently depending on the density. At high ϕ, coarsening occurs after percolation, which happens within the first few τ_B after charge screening by salt. At low ϕ, percolation never takes place and coarsening results in the compaction of individual clusters, which keeps their overall size l_{max}/L, while increasing the number of neighbors $\overline{N}_C$, (see fig. S7). We did not observe any Ostwald ripening among clusters, indicating that the diffusive evaporation-condensation coarsening mechanism is negligible compared to cluster collisions and coalescence, as expected for colloidal viscoelastic phase separation (*16*). At intermediate densities, we observe the process detailed in Fig. 1: formation of low-compacity clusters that then slowly connect together to build the percolating network. This process can take hundreds of τ_B and is competing with cluster compaction, as indicated by the oblique trajectory (red triangles) in Fig. 2B. Particle-level

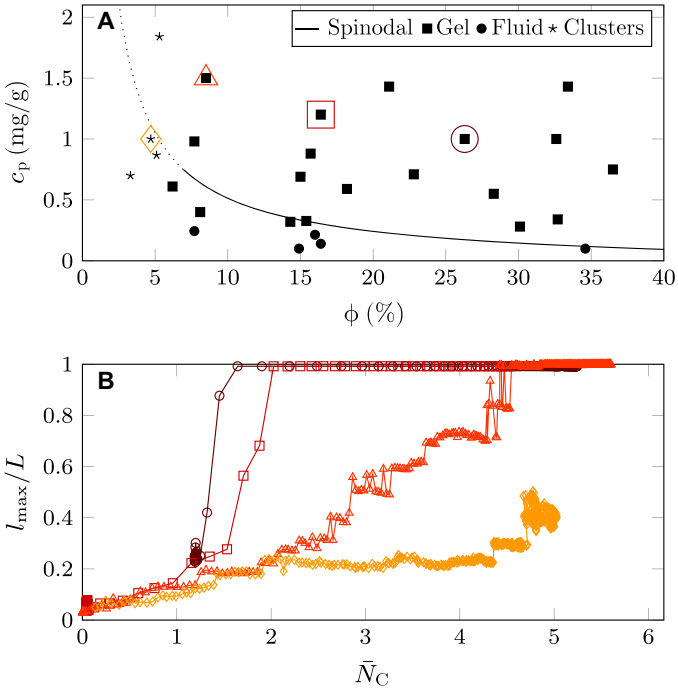

Fig. 2. Different regimes of gelation. (**A**) Phase diagram with respect to colloid volume fraction ϕ and polymer concentration c_p. Black symbols represent experimental points categorized from their final state obtained in the reservoir cell. The spinodal line (solid curve) is obtained from free-volume theory in polymer dilute regime, extended beyond the polymer overlap concentration as a guide for the eye (dotted curve). (**B**) Comparison of system evolution in terms of largest cluster extent (l_{max}/L) and of mean coordination number ($\bar{N}_C$). Symbols ◊, Δ, □, and ○ correspond to (ϕ, c_p) = (4.2%, 1 mg/g), (8%, 1.5 mg/g), (16%, 1.2 mg/g), and (27%, 1 mg/g), respectively, as highlighted in (A).

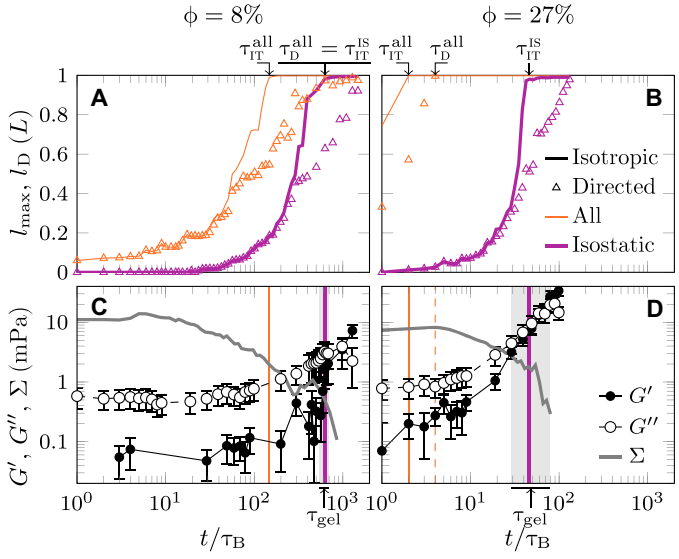

Fig. 3. Evolution of space-spanning microstructure and mechanical response. (**A** and **B**) Percolation processes for a dilute (ϕ = 8%, c_p = 1.5 mg/g) and a dense (ϕ = 27%, c_p = 1 mg/g) sample. The processes of isotropic and directed percolation of all particles are plotted as thin orange curve and orange symbols, respectively. The processes of isotropic and directed percolation of isostatic particles are plotted as thick purple curve and purple symbols, respectively. (**C** and **D**) Mechanical response for the same samples. Elastic (G') and viscous (G'') shear moduli at the highest available frequency ($f = 0.1\tau_B^{-1}$), obtained by two-particle microrheology, are drawn as filled and open circles, respectively. Error bars are obtained following (*71*, *72*). The thick gray curve is the internal stress Σ obtained from the measure of bond-breaking probability (*73*). The thin orange and thick purple vertical lines show the isotropic percolation times for all particles (τ_{IT}^{all}) and isostatic particles (τ_{IT}^{IS}), respectively. The orange dashed vertical line in (D) shows the directed percolation time for all particles (τ_D^{all}). The gray vertical band shows the possible range of mechanical gelation time τ_{gel} (see the Supplementary Materials).

quantities thus demonstrate that the path to gelation is not universal and depends on the colloid volume fraction even within the gelation region. By contrast, polymer concentration, i.e., the depth of the attraction potential, has little effect on the path to gelation (see fig. S6), although rearrangement dynamics never arrests for shallow potentials (*21*). In the next section, we will explore the precise mechanism of arrest and the emergence of mechanical rigidity by studying the dynamics within the network of percolating samples.

Emergence of mechanical stability

Percolation

As already noted by Kohl *et al.* (*23*), the average coordination number $\bar{N}_C$ is a poor predictor of dynamical arrest, as we confirm in fig. S5. In this section, we examine the different percolation time scales and their relation with the emergence of solidity in the samples. In the following, percolation times are noted by the letter τ, with a subscript that labels either isotropic (IT) percolation or directed (D) percolation and a superscript that indicates whether all particles (all) or isostatic particles only (IS) are concerned.

Isotropic percolation is related to the appearance of a system-spanning network and can be determined by looking at the time evolution of the largest connected cluster l_{max}, as plotted in Fig. 3 (A and B) (orange curves). The isotropic percolation time (τ_{IT}^{all}) is then defined as the moment when $l_{max} > 0.95L$. We checked that our field of view is large enough not to suffer from finite size effects.

Directed percolation is related to the appearance of a directed path that spans the whole system. A directed path is defined as a path with no loop or turning back such that every step is in either the positive *X*, *Y*, or *Z* directions. The maximum spatial extent of directed paths l_D is plotted in Fig. 3 (A and B) (orange symbols). We thus define the directed percolation time (τ_D^{all}) as the moment when $l_D > 0.95L$.

The concepts of isotropic and directed percolation can also be applied to a subset of particles. In particular, we focus here on isostatic particles, which are particles that have at least six bonded neighbors. For isostatic clusters, we plot both l_{max} (purple curves) and l_D (purple symbols) in Fig. 3 (A and B) (see also movie S2). The isotropic percolation time of isostatic particles is τ_{IT}^{IS}.

Figure 3 (A and B) shows the time evolution of the clusters in the dilute (ϕ = 8%) (Fig. 3A) and dense suspensions (ϕ = 21%) (Fig. 3B). We observe that directed percolation of all particles and isotropic percolation of isostatic particles occur simultaneously in the dilute regime, $\tau_D^{all} \sim \tau_{IT}^{IS}$. However, the two time scales are well separated in the dense regime, $\tau_D^{all} \ll \tau_{IT}^{IS}$. This separation of the time scales offers the opportunity to test the role of both types of space-spanning microstructures in the mechanical stability of gels.

Mechanical stability and percolations

The solid nature of a material is most often defined from linear mechanical response. For colloidal gels, however, mechanical stability cannot be predicted without an understanding of internal stresses

(*14*). Here, we are able to extract both information from our particle-level experiments. We use the particles themselves as passive microrheological probes to extract the elastic (G') and viscous (G'') parts of the shear modulus (see the Supplementary Materials). Microrheology is a transformation (generalized Stokes-Einstein relation) applied on the (two-point) mean square displacement (*52*). It thus relates dynamical measurements with linear viscoelasticity. In particular, observing $G' > G''$ for a given frequency indicates the emergence of elasticity, or dynamical arrest, at the corresponding time scale. We denote this time as τ_{gel}, the gelling time (see the Supplementary Materials for a more accurate definition and a discussion on uncertainties). We also extract the average value of the internal stress Σ from the bond-breaking rate (see the Supplementary Materials). Results are shown in Fig. 3 (C and D) for direct comparisons with the microstructure.

The typical ranges of stresses and moduli that we measure extend below 0.1 mPa, well below sensitivity of conventional rheometers. That is why previous microscopic studies on the mechanics of colloidal gels have been restricted to the comparison of the structure before and after a large amplitude shear flow with no simultaneous measure of the stress response (*31*, *44*, *53*). From Fig. 3 (C and D), we see that, as expected, all samples are purely viscous at short times, with a value of G'' consistent with the viscosity of a hard sphere suspension at their respective volume fractions. Internal stresses are high at short time, reflecting the stretching of the network, which is formed by hydrodynamic interactions in a mechanically frustrated state. The emergence of mechanical stability is captured simultaneously from both the linear viscoelasticity measurements, with the crossing between G' and G'', and the internal stress, which is accompanied by a sharp drop in Σ. The timing of the emergence of elasticity is thus unambiguous (vertical gray zone in Fig. 3, C and D) and occurs well after isotropic percolation time τ_{IT}^{all} (see orange vertical lines in Fig. 3, C and D). We also find no special value of $\overline{N}_C$ at that time (see fig. S5). This generalizes observations by Kohl *et al.* (*23*) on the final state of dilute samples (see the Supplementary Materials).

In dilute samples, the elastic behavior occurs in the same time scale as directed percolation of all particles. However, isotropic percolation of isostaticity also occurs simultaneously, $\tau_D^{all} \sim \tau_{IT}^{IS} \sim \tau_{gel}$. Therefore, we have to look at the dense regime to disentangle the two possible microstructural causes. In the dense regime, the elastic behavior emerges around $\tau_{gel} \sim 45\tau_B$ well after directed percolation of all particles taking place at $\tau_D^{all} \sim 4\tau_B$. Thus, directed percolation is not generally a sufficient condition to obtain mechanical stability. However, we observe systematically that elasticity emerges in the same time scale as isotropic percolation of isostaticity, $\tau_D^{all} \ll \tau_{IT}^{IS} \sim \tau_{gel}$ (as indicated by the thick purple vertical lines falling inside the gray vertical zone in Fig. 3, C and D). Directed percolation of isostaticity (purple symbols in Fig. 3, A and B) always occurs at later times and does not seem to play an important role. This allows us to reveal the main result of this article: The emergence of rigidity is caused by isotropic percolation of isostatic clusters, able to bear stress across the sample. We show below why the isotropic percolation of isostatic particles occurs at the same time as directed percolation in the dilute regime while being decoupled from it at higher volume fractions.

Directed or isostaticity percolations

In Fig. 4A, we compare the time to percolation of isostaticity τ_{IT}^{IS} ($\sim\tau_{gel}$) to the time to directed percolation τ_D^{all} across all our experiments. We confirm that at high volume fractions, typically $\phi > 14\%$, the two types of percolation phenomena are decoupled, with $2 < \tau_{IT}^{IS}/\tau_D^{all} < 20$ depending on the state point. By contrast, at lower ϕ, both percolations occur simultaneously, independent of the attraction strength.

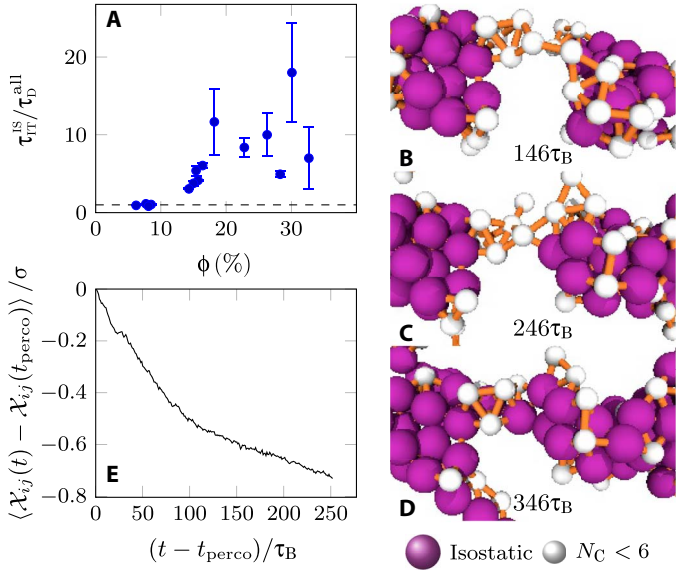

Fig. 4. Directed percolation and isostaticity percolation. (**A**) Ratio of the time of isostaticity percolation τ_{IT}^{IS} to that of directed percolation τ_D^{all}, as a function of colloid volume fraction. Horizontal dashed line shows when both times are equal. (**B**) Detail of a reconstruction from confocal coordinates around the percolation time in a dilute sample (ϕ = 8%, c_p = 1.5 mg/g). Isostatic particles are drawn to scale; non-isostatic ones are drawn smaller for clarity. The bond network is displayed in orange. (**C** and **D**) Same as (B) at later times. (**E**) Increment of Euclidean distance between two isostatic clusters, averaged over all such pairs initially connected by a non-isostatic network strand. The reference time is the percolation time t_{perco}.

The reason for this coincidence can be understood by the specific path to gelation in the dilute regime. We have seen in Fig. 2B that isotropic percolation occurs at a late stage, when the clusters have already become compact by squeezing out the solvent to form isostatic structures. Figure 3A shows that at the percolation time ($\tau_{IT}^{all} \sim 1.5 \times 10^2\tau_B$), isostatic particles already form clusters that reach up to a 10th of the observation window L. Cluster size distribution (see fig. S10) and three-dimensional reconstruction in Fig. 4B show that these isostatic clusters around the percolation time are compact, typically three to five particles in diameter and linked by non-isostatic bridges. The floppiness of these bridges prevents directed paths to reach percolation.

From this situation, percolation of isostaticity proceeds by the compaction of the floppy bridges. This compaction takes place without adsorption of new particles onto the bridge. Compaction is a local process that involves no particle migration but only creation of new bonds, as shown in Fig. 4 (B to D) and sketched in Fig. 5A. Consistently, this compaction leads to a straightening and a shortening of the strands. We quantify this shortening by computing the Euclidean distance $\mathcal{X}_{ij}(t)$ between the centers of mass of two isostatic clusters i and j. The increment of this distance as a function of the time distance to the percolation, averaged over all cluster pairs connected by a floppy bridge, is shown in Fig. 4E. The observed shortening is about 0.7σ or 25% of the initial length. Directed percolation becomes possible only when a percolating path has become straight enough, which implies isostaticity. That is why directed percolation and isostaticity percolation occur simultaneously in the dilute regime. The simultaneity of directed percolation and emergence of rigidity in the dilute regime is thus a coincidence mediated by isotropic percolation of already isostatic clusters, in which

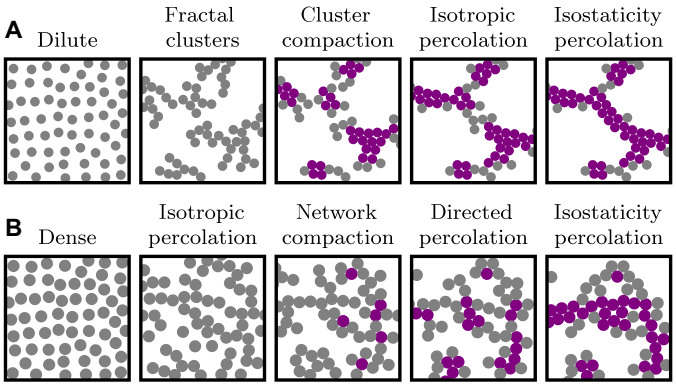

Fig. 5. Sketch of the two possible paths to mechanically stable gel. (**A**) Dilute path. (**B**) Dense path. Isostatic particles are shown in purple; non-isostatic particles are in gray.

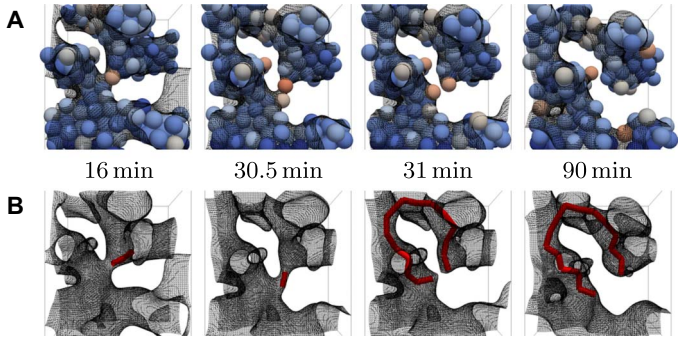

Fig. 6. Breakup of the network by internal stress. (**A**) Reconstruction from experimental coordinates (ϕ = 29%, c_p = 0.7 mg/g) of a strand rupture event. Particles are drawn to scale and colored by a measure of twofold symmetry q_2 (*74*, *75*) (see the Supplementary Materials for its definition) from blue (low) to red (high). We note that q_2 is a measure of the degree of local stretching. (**B**) Same event from a topological point of view. The red line indicates the shortest on-graph path between the two particles of interest, whose drastic change indicates the breakup event. The meshed surface is a Gaussian coarse graining of the network pattern.

the two different types of percolation can take place at the same time. That is, the emergence of rigidity in gels should not be linked to the universality class of directed percolation.

Stress-induced network breakup

In a dense system, after directional percolation of all particles, the number of nearest neighbors monotonically increases to minimize the energy of the structure (mainly the interfacial energy cost), resulting in the growth of isostatic configurations (see Fig. 5B), as discussed above. During this process, the mechanical tension internal to the network grows, driving it toward compaction, which can lead to network coarsening accompanying bond breakage (see Fig. 6, A and B). Unlike in simulations (*13*), we cannot directly measure the local internal stress at this moment, but we can still see its effects through the local stretching measured by the degree of twofold symmetry q_2 (see the particle color in Fig. 6A). From this, we may say that a bond breakage event is the consequence of stress concentration on a weak bond, leading to local stretching of the bond and its eventual breakup. That is, mechanical stress acts against diffusive particle aggregation (or compaction), which is the stress-diffusion coupling characteristic of phase separation in dynamically asymmetric mixtures (*4*, *16*). This stress-driven aging is accompanied by mechanical fracture of the percolated network structure by the self-generated mechanical stress. The mechanical stability can be attained only after the formation of a percolated isostatic structure, which is a necessary and sufficient condition for a structure to be mechanically stable. When the percolated isostatic structure can support the internal stress everywhere, the system can attain mechanical stability.

DISCUSSION

In summary, we have observed with particle-level resolution the entire process of gelation from the very beginning to the final arrested state at various state points. The early stages are characterized by the universal features of spinodal decomposition, with clusters emerging with a constant wave vector (in the Supplementary Materials, we also show that hydrodynamic interactions hinder the formation of isolated compact clusters, leading to the formation of a percolated network, and give a nonuniversal behavior to the coarsening process). At high volume fractions, elongated structures immediately percolate into a thin, mechanically unstable network that undergoes stress-driven rearrangements, enabling the formation of locally isostatic structures that finally percolate (see Fig. 5B). At low volume fractions, percolation is delayed; thus, initially elongated clusters have the time to compact before eventually connecting into a percolating structure (see Fig. 5A). Isostatic clusters thus already exist at the percolation time but are linked by floppy strands that have to compact to induce isostaticity percolation. Microrheological information reveals that the general mechanism responsible for mechanical solidity, which is signaled by the dominance of elastic over viscous modulus, is neither isotropic percolation nor directed percolation but instead the isotropic percolation of isostatic structures.

The picture of gelation that emerges from our observations is far more rich than previously understood and suggests that mechanical stability plays a fundamental role in addition to dynamical arrest. The glass transition is kinetically defined as the point above which the relaxation time is slower than the observation time, whereas mechanical stability is acquired with the percolation of isostaticity. Thus, we argue that a key feature of gelation is the arrest by isostaticity percolation of viscoelastic spinodal decomposition. Then, the mechanical stability of a gel is determined by a competition between the yield stress of the isostaticity network and the internal stress toward network shrinking produced by the interface free-energy cost. Because a gel is not in an equilibrium state and the stress can be concentrated in a weak part of the network, perfect mechanical stability may never be attained, resulting in slow aging via either surface diffusion or bond breakage.

An understanding based on the mechanical equilibrium and isostaticity might pave the way to a more operative description of colloidal gels and allow complex issues to be addressed in terms of mechanics and rheology. For example, stress-driven aging plays a fundamental role in the formation of porous crystals (*49*). Furthermore, an understanding of how hydrodynamic flows affect the microscopic structure of the gel and then how the isostatic network recovers could shed new light on thixotropy (i.e., a reversible decrease in viscosity) in colloidal gels (*54*). The spontaneous delayed collapse of colloidal gels (*55*, *56*) could be viewed as the final step to overcoming the mechanical frustration. In addition, under small stresses, a delayed yielding is observed (*57*–*59*). Despite sustained attention, the yielding process of colloidal gels still lacks a general consensus. For instance, we do not know why some colloidal gels display a yield stress fluid behavior, that is, a reversible yielding and no fracture (*57*, *60*), whereas others display a brittle solid

behavior with the irreversible opening of fractures (*59*). Yielding, with the rapid increase in viscosity and the emergence of elastic behavior, can originate from multiple physical mechanisms. Together with the slowing down of the spontaneous relaxation of the system (as considered in the glassy paradigm of gelation), our work singles out the role of the formation of a network of isostatic particles, suggesting the possibility of a link with the jamming transition (*5*, *61*).

MATERIALS AND METHODS

We used colloidal particles made of poly(methyl methacrylate) copolymerized with 25 kDa methacryloxypropyl-terminated poly(dimethylsiloxane) (Gelest) for steric stabilization (*62*), with 2% of methacrylic acid to allow electrostatic repulsion, and with (rhodamine isothiocyanate)-aminostyrene for fluorescent labeling (*63*). Particles [diameter $\sigma = 2.75$ μm estimated from direct confocal measurements (*64*, *65*)] were dispersed in a mixture of *cis*-decalin (Tokyo Kasei) and bromocyclohexane (Sigma-Aldrich) that matches both the optical index and the density of the colloids (*38*). To induce short-ranged depletion attraction, we used 8.4 MDa polystyrene (Tosoh) as nonadsorbing polymer. We estimated the radius of gyration to $R_g = 148$ nm, leading to an attraction range of $1.10(6)\sigma$. In the absence of salt, the Debye length reaches several micrometers and the (weakly) charged colloids experience a long-range electrostatic repulsion (*66*).

We enclosed this suspension in a thin (200 μm) microscopy cell sketched in fig. S1. The bottom wall of the cell is an osmotic membrane providing contact with a long channel full of the same solvent mixture. At the beginning of the experiment, we introduced solid tetrabutylammonium bromide (Fluka) into the channel and started data acquisition within 30 s. This salt injection screens the electrostatic interactions between colloids. Thus, after the salt injection, the colloid system can be regarded as sticky hard spheres (*67*).

We collected the data on a Leica SP5 confocal microscope, using 532-nm laser excitation. We controlled the temperature of both stage and objective lens, allowing a density matching of the order of 10^{-4} between particles and solvent, enough to observe the late stage of gelation with little influence of gravity despite our large particle size (gravitational Peclet number $Pe < 10^{-6}$). We tracked the particle coordinates in three dimensions with an accuracy of around 0.03σ (*68*). We considered two particles bonded when their distance was shorter than the first minimum of $g(r)$, i.e., 3.55 μm. This defines the bond graph that we analyzed using NetworkX library (*69*). The precise choice of this distance does not significantly affect our results, in particular percolation times (see fig. S4). A discussion of different criteria for defining a bond [e.g., (*70*)] is reported in the Supplementary Materials.

SUPPLEMENTARY MATERIALS

Supplementary material for this article is available at http://advances.sciencemag.org/cgi/content/full/5/5/eaav6090/DC1

Supplementary Text

Fig. S1. Reservoir cell.

Fig. S2. Temporal change of the structure factor.

Fig. S3. Temporal change in the characteristic wave number $\langle q \rangle$.

Fig. S4. Robustness of the bond network used in percolation analysis.

Fig. S5. Coordination number analysis for a dilute and a dense sample.

Fig. S6. Gelation path dependence on polymer concentration.

Fig. S7. Cluster phase formation observed by our method.

Fig. S8. Role of hydrodynamics on colloidal phase separation.

Fig. S9. Temporal change in loss angle.

Fig. S10. Cluster size distributions at respective percolation times.

Movie S1. Reconstructions from confocal coordinates of the whole process of gelation at $\phi = 7.7\%$, $c_p = 1$ mg/g.

Movie S2. Reconstructions in a thin slice from confocal coordinates of the whole process of gelation at $\phi = 27\%$, $c_p = 1$ mg/g.

REFERENCES AND NOTES

1. R. Piazza, G. D. Pietro, Phase separation and gel-like structures in mixtures of colloids and surfactant. *Europhys. Lett.* **28**, 445–450 (1994).
2. H. Verduin, J. K. G. Dhont, Phase diagram of a model adhesive hard-sphere dispersion. *J. Colloid Interface Sci.* **172**, 425–437 (1995).
3. N. A. M. Verhaegh, J. S. van Duijneveldt, J. K. Dhont, H. N. W. Lekkerkerker, Fluid-fluid phase separation in colloid-polymer mixtures studied with small angle light scattering and light microscopy. *Phys. A* **230**, 409–436 (1996).
4. H. Tanaka, Viscoelastic model of phase separation in colloidal suspensions and emulsions. *Phys. Rev. E* **59**, 6842–6852 (1999).
5. V. Trappe, V. Prasad, L. Cipelletti, P. N. Segre, D. A. Weitz, Jamming phase diagram for attractive particles. *Nature* **411**, 772–775 (2001).
6. W. C. K. Poon, The physics of a model colloid–polymer mixture. *J. Phys. Condens. Matter* **14**, R859–R880 (2002).
7. F. Cardinaux, T. Gibaud, A. Stradner, P. Schurtenberger, Interplay between spinodal decomposition and glass formation in proteins exhibiting short-range attractions. *Phys. Rev. Lett.* **99**, 118301 (2007).
8. P. J. Lu, E. Zaccarelli, F. Ciulla, A. B. Schofield, F. Sciortino, D. A. Weitz, Gelation of particles with short-range attraction. *Nature* **453**, 499–503 (2008).
9. A. Onuki, *Phase Transition Dynamics* (Cambridge Univ. Press, 2002).
10. L. Cipelletti, S. Manley, R. C. Ball, D. A. Weitz, Universal aging features in the restructuring of fractal colloidal gels. *Phys. Rev. Lett.* **84**, 2275–2278 (2000).
11. L. Ramos, L. Cipelletti, Ultraslow dynamics and stress relaxation in the aging of a soft glassy system. *Phys. Rev. Lett.* **87**, 245503 (2001).
12. B. Ruta, O. Czakkel, Y. Chushkin, F. Pignon, R. Nervo, F. Zontone, M. Rinaudo, Silica nanoparticles as tracers of the gelation dynamics of a natural biopolymer physical gel. *Soft Matter* **10**, 4547–4554 (2014).
13. H. Tanaka, T. Araki, Spontaneous coarsening of a colloidal network driven by self-generated mechanical stress. *Europhys. Lett.* **79**, 58003 (2007).
14. M. Bouzid, J. Colombo, L. V. Barbosa, E. Del Gado, Elastically driven, intermittent microscopic dynamics in soft solids. *Nat. Commun.* **8**, 15846 (2016).
15. P. Chaudhuri, L. Berthier, Ultra-long-range dynamic correlations in a microscopic model for aging gels. *Phys. Rev. E* **95**, 060601 (2017).
16. H. Tanaka, Viscoelastic phase separation. *J. Phys. Condens. Matter* **12**, R207–R264 (2000).
17. A. Furukawa, H. Tanaka, Key role of hydrodynamic interactions in colloidal gelation. *Phys. Rev. Lett.* **104**, 245702 (2010).
18. Z. Varga, G. Wang, J. W. Swan, The hydrodynamics of colloidal gelation. *Soft Matter* **11**, 9009–9019 (2015).
19. J. Colombo, E. Del Gado, Self-assembly and cooperative dynamics of a model colloidal gel network. *Soft Matter* **10**, 4003–4015 (2014).
20. V. Testard, L. Berthier, W. Kob, Intermittent dynamics and logarithmic domain growth during the spinodal decomposition of a glass-forming liquid. *J. Chem. Phys.* **140**, 164502 (2014).
21. R. N. Zia, B. J. Landrum, W. B. Russel, A micro-mechanical study of coarsening and rheology of colloidal gels: Cage building, cage hopping, and Smoluchowski's ratchet. *J. Rheol.* **58**, 1121–1157 (2014).
22. C. P. Royall, J. Eggers, A. Furukawa, H. Tanaka, Probing colloidal gels at multiple length scales: The role of hydrodynamics. *Phys. Rev. Lett.* **114**, 258302 (2015).
23. M. Kohl, R. F. Capellmann, M. Laurati, S. U. Egelhaaf, M. Schmiedeberg, Directed percolation identified as equilibrium pre-transition towards non-equilibrium arrested gel states. *Nat. Commun.* **7**, 11817 (2016).
24. N. E. Valadez-Pérez, Y. Liu, A. P. R. Eberle, N. J. Wagner, R. Castañeda-Priego, Dynamical arrest in adhesive hard-sphere dispersions driven by rigidity percolation. *Phys. Rev. E* **88**, 060302 (2013).
25. J. J. Richards, J. B. Hipp, J. K. Riley, N. J. Wagner, P. D. Butler, Clustering and percolation in suspensions of carbon black. *Langmuir* **33**, 12260–12266 (2017).
26. C. P. Royall, S. R. Williams, T. Ohtsuka, H. Tanaka, Direct observation of a local structural mechanism for dynamic arrest. *Nat. Mater.* **7**, 556–561 (2008).
27. J. P. Bouchaud, E. Pitard, Anomalous dynamical light scattering in soft glassy gels. *Eur. Phys. J. E Soft Matter* **9**, 287–291 (2002).
28. L. Cipelletti, L. Ramos, S. Manley, E. Pitard, D. A. Weitz, E. E. Pashkovski, M. Johansson, Universal non-diffusive slow dynamics in aging soft matter. *Faraday Discuss.* **123**, 237–251 (2003).

29. D. J. Jacobs, M. F. Thorpe, Generic rigidity percolation: The pebble game. *Phys. Rev. Lett.* **75**, 4051–4054 (1995).
30. S. Zhang, L. Zhang, M. Bouzid, D. Z. Rocklin, E. Del Gado, X. Mao, Correlated rigidity percolation and colloidal gels. arxiv:1807.08858 [cond-mat.soft] (23 July 2018).
31. L. C. Hsiao, R. S. Newman, S. C. Glotzer, M. J. Solomon, Role of isostaticity and load-bearing microstructure in the elasticity of yielded colloidal gels. *Proc. Natl. Acad. Sci. U.S.A.* **109**, 16029–16034 (2012).
32. J. C. Maxwell, L. On the calculation of the equilibrium and stiffness of frames. *Philos. Mag. A* **27**, 294–299 (2009).
33. R. Blumenfeld, S. F. Edwards, R. C. Ball, Granular matter and the marginal rigidity state. *J. Phys. Condens. Matter* **17**, S2481–S2487 (2005).
34. V. J. Anderson, H. N. Lekkerkerker, Insights into phase transition kinetics from colloid science. *Nature* **416**, 811–815 (2002).
35. E. Zaccarelli, Colloidal gels: Equilibrium and non-equilibrium routes. *J. Phys. Condens. Matter* **19**, 323101 (2007).
36. P. N. Pusey, W. Van Megen, Phase behaviour of concentrated suspensions of nearly hard colloidal spheres. *Nature* **320**, 340–342 (1986).
37. D. Bonn, H. Tanaka, G. Wegdam, H. Kellay, J. Meunier, Aging of a colloidal Wigner glass. *Europhys. Lett.* **45**, 52–57 (1999).
38. C. L. Klix, C. P. Royall, H. Tanaka, Structural and dynamical features of multiple metastable glassy states in a colloidal system with competing interactions. *Phys. Rev. Lett.* **104**, 165702 (2010).
39. K. N. Pham, A. M. Puertas, J. Bergenholtz, S. U. Egelhaaf, A. Moussad, P. N. Pusey, A. B. Schofield, M. E. Cates, M. Fuchs, W. C. Poon, Multiple glassy states in a simple model system. *Science* **296**, 104–106 (2002).
40. H. Tanaka, J. Meunier, D. Bonn, Nonergodic states of charged colloidal suspensions: Repulsive and attractive glasses and gels. *Phys. Rev. E* **69**, 031404 (2004).
41. F. A. M. Marques, R. Angelini, G. Ruocco, B. Ruzicka, Isotopic effect on the gel and glass formation of a charged colloidal clay: Laponite. *J. Phys. Chem. B* **121**, 4576–4582 (2017).
42. C. P. Royall, S. R. Williams, H. Tanaka, Vitrification and gelation in sticky spheres. *J. Chem. Phys.* **148**, 044501 (2018).
43. C. O. Osuji, C. Kim, D. A. Weitz, Shear thickening and scaling of the elastic modulus in a fractal colloidal system with attractive interactions. *Phys. Rev. E* **77**, 060402 (2008).
44. S. B. Lindström, T. E. Kodger, J. H. B. Sprakel, D. A. Weitz, Structures, stresses, and fluctuations in the delayed failure of colloidal gels. *Soft Matter* **8**, 3657 (2012).
45. N. Koumakis, E. Moghimi, R. Besseling, W. C. Poon, J. F. Brady, G. Petekidis, Tuning colloidal gels by shear. *Soft Matter* **11**, 4640–4648 (2015).
46. E. Moghimi, A. R. Jacob, N. Koumakis, G. Petekidis, Colloidal gels tuned by oscillatory shear. *Soft Matter* **13**, 2371–2383 (2017).
47. H. Tanaka, Y. Nishikawa, T. Koyama, Network-forming phase separation of colloidal suspensions. *J. Phys. Condens. Matter* **17**, L143–L153 (2005).
48. J. Sato, V. Breedveld, Transient rheology of solvent-responsive complex fluids by integrating microrheology and microfluidics. *J. Rheol.* **50**, 1–19 (2006).
49. H. Tsurusawa, J. Russo, M. Leocmach, H. Tanaka, Formation of porous crystals via viscoelastic phase separation. *Nat. Mater.* **16**, 1022–1028 (2017).
50. P. J. Lu, J. C. Conrad, H. M. Wyss, A. B. Schofield, D. A. Weitz, Fluids of clusters in attractive colloids. *Phys. Rev. Lett.* **96**, 028306 (2006).
51. G. J. Fleer, R. Tuinier, Analytical phase diagrams for colloids and non-adsorbing polymer. *Adv. Colloid Interface Sci.* **143**, 1–47 (2008).
52. J. C. Crocker, M. T. Valentine, E. R. Weeks, T. Gisler, P. D. Kaplan, A. G. Yodh, D. A. Weitz, Two-point microrheology of inhomogeneous soft materials. *Phys. Rev. Lett.* **85**, 888–891 (2000).
53. P. A. Smith, G. Petekidis, S. U. Egelhaaf, W. C. K. Poon, Yielding and crystallization of colloidal gels under oscillatory shear. *Phys. Rev. E* **76**, 041402 (2007).
54. D. Bonn, M. M. Denn, L. Berthier, T. Divoux, S. Manneville, Yield stress materials in soft condensed matter. *Rev. Mod. Phys.* **89**, 035005 (2017).
55. S. W. Kamp, M. L. Kilfoil, Universal behaviour in the mechanical properties of weakly aggregated colloidal particles. *Soft Matter* **5**, 2438–2447 (2009).
56. P. Bartlett, L. J. Teece, M. A. Faers, Sudden collapse of a colloidal gel. *Phys. Rev. E* **85**, 021404 (2012).
57. T. Gibaud, D. Frelat, S. Manneville, Heterogeneous yielding dynamics in a colloidal gel. *Soft Matter* **6**, 3482–3488 (2010).
58. J. H. B. Sprakel, S. B. Lindström, T. E. Kodger, D. A. Weitz, Stress enhancement in the delayed yielding of colloidal gels. *Phys. Rev. Lett.* **106**, 248303 (2011).
59. M. Leocmach, C. Perge, T. Divoux, S. Manneville, Creep and fracture of a protein gel under stress. *Phys. Rev. Lett.* **113**, 038303 (2014).
60. V. Grenard, T. Divoux, N. Taberlet, S. Manneville, Timescales in creep and yielding of attractive gels. *Soft Matter* **10**, 1555–1571 (2014).
61. A. J. Liu, S. R. Nagel, Jamming is not just cool any more. *Nature* **396**, 21–22 (1998).
62. S. M. Klein, V. N. Manoharan, D. J. Pine, F. F. Lange, Preparation of monodisperse PMMA microspheres in nonpolar solvents by dispersion polymerization with a macromonomeric stabilizer. *Colloid Polym. Sci.* **282**, 7–13 (2003).
63. G. Bosma, C. Pathmamanoharan, E. H. A. de Hoog, W. K. Kegel, A. van Blaaderen, H. N. Lekkerkerker, Preparation of monodisperse, fluorescent PMMA-latex colloids by dispersion polymerization. *J. Colloid Interface Sci.* **245**, 292–300 (2002).
64. C. P. Royall, A. A. Louis, H. Tanaka, Measuring colloidal interactions with confocal microscopy. *J. Chem. Phys.* **127**, 044507 (2007).
65. W. C. K. Poon, E. R. Weeks, C. P. Royall, On measuring colloidal volume fractions. *Soft Matter* **8**, 21–30 (2012).
66. C. P. Royall, M. E. Leunissen, A. v. Blaaderen, A new colloidal model system to study long-range interactions quantitatively in real space. *J. Phys. Condens. Matter* **15**, S3581–S3596 (2003).
67. A. I. Campbell, V. J. Anderson, J. S. van Duijneveldt, P. Bartlett, Dynamical arrest in attractive colloids: The effect of long-range repulsion. *Phys. Rev. Lett.* **94**, 208301 (2005).
68. M. Leocmach, *Colloids* (2009); http://doi.org/10.5281/zenodo.31286.
69. A. A. Hagberg, D. A. Schult, P. J. Swart, Exploring network structure, dynamics, and function using NetworkX, *Proc. SciPy* **836**, 11–15 (2008).
70. B. D. Leahy, N. Y. C. Lin, I. Cohen, Quantitative light microscopy of dense suspensions: Colloid science at the next decimal place. *Curr. Opin. Colloid Interface Sci.* **34**, 32–46 (2018).
71. T. Savin, P. S. Doyle, Static and dynamic errors in particle tracking microrheology. *Biophys. J.* **88**, 623–638 (2005).
72. F. Chambon, H. H. Winter, Linear viscoelasticity at the gel point of a crosslinking PDMS with imbalanced stoichiometry. *J. Rheol.* **31**, 683–697 (1987).
73. H. A. Kramers, Brownian motion in a field of force and the diffusion model of chemical reactions. *Phys. Ther.* **7**, 284–304 (1940).
74. P. J. Steinhardt, D. R. Nelson, M. Ronchetti, Bond-orientational order in liquids and glasses. *Phys. Rev. B* **28**, 784–805 (1983).
75. M. Leocmach, *Pyboo* (2017); http://doi.org/10.5281/zenodo.1066568.

Acknowledgments

Funding: This study was partly supported by Grants-in-Aid for Scientific Research (A) (JP18H03675) and Specially Promoted Research (JP25000002) from the Japan Society for the Promotion of Science (JSPS). Collaboration between M.L. and H.Ta. has been funded by CNRS through Projet International de Coopération Scientifique no. 7464. M.L. acknowledges support from ANR grant GelBreak ANR-17-CE08-0026. J.R. acknowledges support from the European Research Council (grant DLV-759187) and the Royal Society University Research Fellowship. **Author contributions:** H.Ta. conceived and supervised the project. H.Ts. performed experiments. M.L. performed most of the analysis of the experimental coordinates. J.R. performed simulations. All authors discussed and M.L., J.R., and H.Ta. wrote the manuscript. **Competing interests:** The authors declare that they have no competing interests. **Data and materials availability:** All data needed to evaluate the conclusions in the paper are present in the paper and/or the Supplementary Materials. Additional data related to this paper may be requested from the authors.

Submitted 3 October 2018
Accepted 23 April 2019
Published 31 May 2019
10.1126/sciadv.aav6090

Citation: H. Tsurusawa, M. Leocmach, J. Russo, H. Tanaka, Direct link between mechanical stability in gels and percolation of isostatic particles. *Sci. Adv.* **5**, eaav6090 (2019).

Direct link between mechanical stability in gels and percolation of isostatic particles

Hideyo Tsurusawa, Mathieu Leocmach, John Russo and Hajime Tanaka

Sci Adv **5** (5), eaav6090.
DOI: 10.1126/sciadv.aav6090